# Inductance effects and dimensionality crossover in hybrid superconducting arrays

H. R. Shea, M. A. Itzler, and M. Tinkham
*Department of Physics and Division of Applied Sciences, Harvard University, Cambridge, Massachusetts 02138*
(Received 8 December 1994)

We report measurements made on hybrid arrays consisting of superconducting wires along one direction of a square geometry and Josephson junctions along the perpendicular direction. The differential resistance $R_d$ across the array as a function of normalized applied flux per plaquette $f=\Phi/\Phi_0$ exhibits two distinct types of behavior. When the ratio $\beta \equiv L_g/L_J$ of the geometric inductance of an array plaquette to the Josephson-junction inductance is much less than unity, we observe oscillations in $R_d$ characteristic of a one-dimensional (1D) $N$-junction interferometer. However, as $\beta$ approaches 1, the simultaneous suppression of interferometer oscillations and emergence of local minima in $R_d$ at commensurate fields $f=p/q$ (where $p$ and $q$ are integers) signal a crossover to behavior typical of 2D superconducting arrays. To model the experimental system, we have performed simulations of 2D arrays of Josephson junctions made anisotropic by incorporating different coupling in the two perpendicular directions (i.e., anisotropic $XY$ model). In the limit of large anisotropy we find 1D interferometer behavior; as the anisotropy is reduced, we see a crossover to the 2D behavior familiar in isotropic arrays.

## I. INTRODUCTION

Arrays of superconducting junctions and wires provide excellent experimental models for investigating many general physical concepts including frustration, commensurability, localization, and phase transitions in two dimensions. They have also generated intense interest in their possible application as practical devices such as high-frequency detectors and sources, flux-flow transistors, and interferometric magnetic-flux detectors. In this paper, we describe a set of experimental results which provides new insights in two areas of current interest. First, there have been a number of studies undertaken to investigate the effects of anisotropy both theoretically[1–3] and experimentally[4] in various types of superconducting arrays. These investigations of anisotropy in two dimensions complement the extensive interest in anisotropic layered materials following the discovery of high-$T_c$ copper oxides. Second, there has been extensive work demonstrating the effects of self- and mutual inductances of the individual cells of superconducting arrays.[5–9] These results are especially important with respect to understanding the dynamic behavior of arrays.

In order to study systems in the limit of extreme anisotropy, we have fabricated "hybrid" arrays with superconducting wires along one direction of a square geometry and Josephson weak links along the perpendicular direction [Fig. 1(a)]. Our measurements indicate that these devices exhibit either one-dimensional (1D) or two-dimensional (2D) behavior depending on the magnitude of the inductances of the superconducting wires compared to the Josephson inductances of the weak links. Since the latter are strongly temperature dependent while the former are not, the hybrid geometry displays a clear crossover in the dimensional behavior of the system as its temperature is varied.

The essential physics of superconducting arrays in a magnetic field lies in the single valuedness of the complex order parameter. This requires the total winding of the phase of the order parameter around any closed loop to be an integral multiple of $2\pi$, with contributions coming from applied and induced fields and currents. Loops with phase windings of $2\pi n$ (for $n$ an integer) are said to contain $n$ magnetic-flux quanta, and the field-dependent array behavior is often conveniently described in terms of a superlattice of vortices each containing a single quantum of flux. In particular, the collective vortex behavior is the result of competing interactions due to the mutual repulsion between vortices and their attraction to potential minima in the geometry of the array. At fractional fillings $p/q$ (where $p$ and $q$ are integers), these interactions can be more favorably resolved than at nearby incommensurate fillings, giving rise to local extrema in the values of many properties of the arrays (e.g., critical current and superconducting–normal transition temperature). These extrema are the signatures of commensurate states for which the lattice of vortices is locked to the ar-

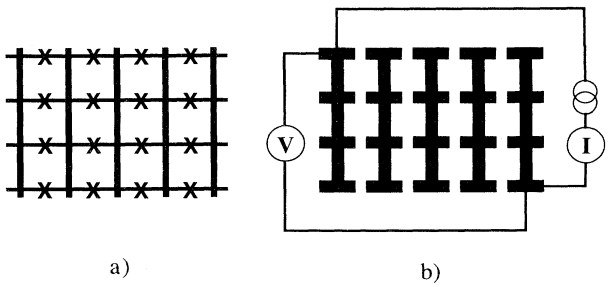


FIG. 1. (a) Schematic diagram of a 4 by 3 plaquette (5 wire by 4 junction) hybrid array. The junctions are represented by crosses and the wires by solid line. (b) Geometry of the niobium film after patterning. The niobium is deposited on a copper substrate (not shown) to form an array isomorphic to (a). The four-probe measurement is made as indicated.

 ©1995 The American Physical Society

ray geometry in a stable configuration, and they are characteristic of 2D systems. In particular, it is generally believed that the commensurate configurations of a square geometry can be described[10] by the repetition of a pattern of $p \times q$ vortices arranged on each $q \times q$ supercell (or at least small $q$).

1D ladder geometries are not expected to show such commensurate structure at fractional fillings. Simulations of 1D ladders for which the "rungs" are continuous wires[11] exhibit commensurate behavior only at integral fillings of the arrays (i.e., fields for which every plaquette has the same number of vortices) and never at fractional fillings. On the other hand, a system of $N$ weak links in parallel (i.e., a ladder with weak links on the rungs) exhibits the same behavior as an optical interferometer with $N$ slits as far as its "transmission" (i.e., current-carrying) properties are concerned. The structure found in the dependence of the 1D array properties on the applied field is quite distinct from the 2D commensurate states referred to above.

Our results indicate that the presence or absence of commensurate structure in hybrid arrays is closely tied to where phase differences are present in the system. When the phase differences in our hybrid arrays occur predominantly across the weak links, the phase topology of the system is equivalent to that of independent $N$-junction interferometers in series and the behavior of the system is consistent with this 1D geometry. However, at low temperatures, where the loop currents can be much larger, phase gradients along the wires become considerable as well, and the properties of the system then reflect the 2D nature of the phase gradients. To support our experimental results and interpretation, we have simulated the hybrid arrays using an anisotropic version of the $XY$ model by modeling the phase gradients along the wires with localized phase drops across weak links. The simulation results exhibit behavior very similar to the experimental data, namely the existence of a crossover between 1D and 2D behavior as phase differences become comparable in the two directions.

We should also mention that the very sensitive dependence of interferometer properties on an applied magnetic field suggests the potential application of our devices as multijunction superconducting quantum interference devices. For the usual 1D interferometer, the enhancement of field sensitivity gained by increasing the number of junctions used in parallel is necessarily accompanied by a proportionally decreased resistance and hence a decreased signal level. However, our hybrid geometry (in its 1D limit) allows the same increase in sensitivity while maintaining the signal level due to its equivalence to many identical interferometers in series. Thermally induced flux noise in this system will be dictated by a single loop area, and the presence of many loops should provide substantial averaging of this noise over the entire area.

In the next section, we review the theoretical description of superconducting loops in a magnetic field. Then experimental details and results are presented in Secs. III and IV, respectively. Section V contains the numerical simulations, and in Sec. VI we discuss our results. Our conclusions are summarized in Sec. VII.

## II. THEORETICAL BACKGROUND

Because the superconducting order parameter $|\psi|e^{i\varphi}$ must be single valued, its phase $\varphi$ is required to wind by an integral multiple of $2\pi$ along any closed loop of superconducting material:

$$\oint \nabla\varphi \cdot dl = 2\pi n \ , \tag{1}$$

where $n$ is an integer. If we rewrite $\nabla\varphi$ in terms of the current density $\mathbf{J}$ and magnetic vector potential $\mathbf{A}$ along the loop, Eq. (1) leads to

$$\frac{2\pi}{\Phi_0}\oint \mu_0\lambda^2\mathbf{J}\cdot dl + \frac{2\pi}{\Phi_0}\oint \mathbf{A}\cdot dl = 2\pi n \ , \tag{2}$$

where $\lambda$ is the bulk penetration depth of the superconductor and $\mu_0$ is the magnetic permeability of free space, and the flux quantum $\Phi_0 = \hbar/2e = 2.07\times10^{-15}$ Wb. This constraint, known as fluxoid quantization, is central in governing the behavior of multiply connected superconductors in a magnetic field. We can generalize this condition by including the possibility of phase differences $\Delta\varphi$ at weak links in the loop:

$$\oint \mu_0\lambda^2\mathbf{J}\cdot dl + \Phi + \frac{\Phi_0}{2\pi}\sum_m \Delta\varphi_m = n\Phi_0 \ , \tag{3}$$

where the sum is over the weak links in the loop and we have made use of the fact that $\oint \mathbf{A}\cdot dl = \int \mathbf{B}\cdot dS$ is just the flux $\Phi$ through the loop.

We can simplify Eq. (3) further if we assume an isolated superconducting wire loop of cross section $A$ and circumference $l$ along which $\lambda$ is constant and around which a current $I$ is flowing. We also assume an arbitrary number of identical weak links with critical current $i_c$ for which the current-phase (Josephson) relation is $I = i_c\sin(\Delta\varphi)$. Further, noting that the net flux $\Phi$ is the sum of the applied flux $\Phi_{\text{app}}$ and the flux $\Phi_{\text{ind}}$ induced by the circulating current, we obtain

$$\begin{aligned} n\Phi_0 - \Phi_{\text{app}} &= \mu_0\lambda^2\mathbf{J}l + \Phi_{\text{ind}} + \frac{\Phi_0}{2\pi}\sum_m \sin^{-1}\left[\frac{I}{i_c}\right] \\ &\cong L_k I + L_g I + \sum_m L_J I \ , \end{aligned} \tag{4}$$

where the sum is over all weak links and in the final form we make the linear approximation $\sin^{-1}x \cong x$ to emphasize the similar role played by each of these inductances. Equation (4) reflects that the phase gradient induced by the difference of the applied flux $\Phi_{\text{app}}$ from an integral number of flux quanta $n\Phi_0$ must be made up by the three inductive terms on the right-hand side: $L_k \equiv (\mu_0\lambda^2)(l/A)$ is the kinetic inductance of the loop, $L_g$ is the geometric self-inductance of the loop, and $L_J \equiv \Phi_0/(2\pi i_c)$ is the Josephson inductance of the weak links.

We can examine two specific applications of Eq. (4). First, consider the case of no weak links ($L_J = 0$). The kinetic inductance $L_k \propto \lambda^2$ diverges near $T_c$ of the wires, in which case the difference $n\Phi_0 - \Phi_{\text{app}}$ is balanced by $L_k I$ with only a very small current $I$ and therefore practi-

cally no induced flux $\Phi_{\rm ind}=L_g I$. However, in general the geometric inductance per unit length $L_g/l \approx \mu_0 \ln(s/r)$, where $s$ is the radius of the loop formed by the wire of radius $r$, and so $L_g/l$ will be of order $\mu_0$. Since $L_k/l=\mu_0\lambda^2/A \approx \mu_0(\lambda/r)^2$ and $\lambda \ll r$ for $\mu$m-scale samples at temperatures not near $T_c$, we will always have $L_g \gg L_k$ except very near $T_c$.

When weak links are present, we must consider the ratio $\beta \equiv L_g/L_J = 2\pi L_g i_c/\Phi_0$. For sufficiently small $i_c$ ($\beta \ll 1$), the Josephson term in Eq. (4) dominates, and we can neglect the induced flux. However, as $i_c$ approaches $\Phi_0/2\pi L_g$ (i.e., as $\beta \to 1$), the phase winding due to the induced flux $L_g I$ is comparable to the phase drops across the junctions and can no longer be ignored. Note that $\beta=2\pi$ when the maximum induced flux $L_g i_c$ is equal to $\Phi_0$.

A collection of loops in an array exhibits much more complicated behavior due to effects such as frustration arising from shared links between loops and mutual inductances between loops. Nevertheless, we find that the various inductances for a single loop in Eq. (4) still play similar roles in this more complex system. For the reasons described earlier, the kinetic inductance $L_k$ will still be negligible for $\mu$m-scale loops, and so the relationship between $L_g$ and $L_J$ will be central in determining the behavior of the array.

## III. EXPERIMENTAL DETAILS

Our experimental samples consist of a 2500 Å thick Cu film beneath 2500 Å of Nb patterned to form superconducting wires in one direction and superconducting–normal-metal–superconducting (SNS) Josephson junctions in the perpendicular direction [see Fig. 1(b)]. After depositing the underlying normal-metal layer, the wafer is repatterned to define the array geometry. The Cu surface is Ar ion etched immediately prior to dc magnetron sputtering of Nb followed by a final liftoff. The lattice spacing for the square geometry is 10 $\mu$m, the junction width is 2 $\mu$m, and the gap between the superconducting electrodes which form the junctions is 2.2 $\mu$m. On each wafer we simultaneously fabricate square arrays consisting of 10×10, 20×20, 40×40, 80×80, and 400×400 plaquettes, as well as single Josephson junctions. Each plaquette of the hybrid arrays is formed by two junctions along with the superconducting wires which connect them.

Measurements were made using standard four-probe techniques. Figure 1(b) shows our usual lead configuration, in which the current is injected on one end of the first wire and extracted from the opposite end of the last wire. To measure the differential resistance $R_d \equiv dV/dI$, we used a PAR 5302 lock-in amplifier operating at 28.86 Hz with rms current ranging from 1 to 50 $\mu$A; using a 1:100 coupling transformer, typical sensitivities were about 200 pV. To suppress digital noise from the lock-in and from the computer controlling the data acquisition process, we used room temperature LC low-pass (Erie) filters on all leads to the samples.

The arrays were cooled to 350 mK in a $^3$He cryostat enclosed within a double $\mu$-metal shield which reduced the stray fields to less than 50 mG. The temperature was controllable to above the Nb transition temperature and stable to ±3 mK below 2 K. Perpendicular fields were applied to the sample using a solenoid surrounding the vacuum can of the cryostat, and dc currents $I_{\rm dc}$ were superimposed on the ac bias allowing us to measure $R_d(H, I_{\rm dc})$ at various temperatures.

The transition temperature of the niobium was 8.3 K. In zero magnetic field, the asymptotic resistance of the square arrays for $I_{\rm dc} \gg I_c$ measured with the same lead configuration as in Fig. 1(b) was approximately 4 mΩ at 2 K. Single SNS junctions had negligible capacitance, very small resistance (a few mΩ), and were nonhysteretic. Their critical current $i_c$ was a strong function of temperature $T$. For overdamped SNS junctions, de Gennes[12] derived that

$$i_c = I_0 \left[1-\frac{T}{T_{\rm BCS}}\right]^2 \exp[-d/\xi_N(T)] ,$$

where $d$ is the separation between the superconducting electrodes, $T_{\rm BCS}$ is the bulk transition temperature, $I_0$ is the zero-temperature critical current and $\xi_N = \sqrt{\hbar v_N l_N/6\pi k_B T}$ is the dirty-limit normal-metal coherence length ($l_N \sim 200$ Å and $v_N \sim 1.6\times10^6$ m/s are the mean free path and Fermi velocity, respectively). The data for $I_c(T)$ of the arrays in zero field fit this temperature dependence well, with $\xi_N(T=1\ {\rm K}) \approx 2400$ Å.

## IV. EXPERIMENTAL RESULTS

Figure 2 shows the zero-field dynamic resistance $R_d$ as a function of dc current $I_{\rm dc}$ for a 20×20 plaquette hybrid array for temperatures between 0.8 and 1.4 K at 0.1 K intervals. We take the array critical current $I_c$ to be that current corresponding to the peaks in $R_d$ as is usual for single junctions.[13] Extracting the single junction critical current $i_c$ using $i_c = I_c/21$ (for an array width of 21 junctions), we find $i_c$ varies from 1.7 $\mu$A at 1.6 K to 21 $\mu$A at 0.8 K.[14] For measurements made in the resistive regime

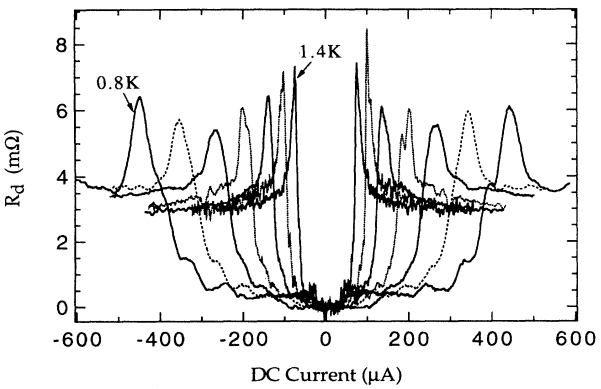


FIG. 2. Measured dynamic resistance $R_d$ as a function of dc current $I_{\rm dc}$ for a 20 by 20 plaquette hybrid array at temperatures ranging from 0.8 to 1.4 K in 0.1 K intervals in zero magnetic field.

(in which case vortices are flowing across the array), we can assume uniform field penetration and current flow (at least in a time-averaged sense).

Figure 3 shows a plot of $R_d(f)$ (where $f=\Phi/\Phi_0$ is the normalized applied flux per plaquette) for three different array sizes for $\beta=0.08$ (corresponding to a temperature of 1.6 K). The observed structure is essentially that of an $N$-junction interferometer (note that along a given column of the array, $N$ junctions form $N$-1 plaquettes), in which the total current crossing the device is

$$I(f,\gamma_0)=\sum_{n=0}^{N-1} i_c \sin(2\pi n f+\gamma_0)\ , \tag{5}$$

where $\gamma_0$ is the (arbitrary) phase difference across the lower-most junction and $i_c$ is the single-junction critical current, and in which the field is assumed to be uniform (i.e., the geometric inductances are equal to zero). Maximizing the current at any given field yields the field-dependent critical current

$$I_c(f)=i_c\left|\frac{\sin(N\pi f)}{\sin(\pi f)}\right|\ . \tag{6}$$

This dependence is illustrated for $N=11$ by the dotted curve in Fig. 4.

Consider the field-dependent resistance $R(f)$ of an ideal interferometer at zero temperature measured with a bias current of small amplitude $I_{\rm bias}<i_c$. The oscillations of $I_c(f)$ above and below $I_{\rm bias}$ lead to pulselike sharp transitions in $R(f)$ between zero resistance and the normal-state resistance $R_N$. As can readily be seen from the plot of $I_c(f)$ in Fig. 4 (dotted line), the maximum value of $I_{\rm bias}$ that will still modulate $R(f)$ for every local maximum of $I_c(f)$ is $I_{\rm bias}=i_c$. At finite temperatures, the sudden jump from zero resistance to $R_N$ at $I=I_c$ is replaced by a more gradual transition (as dictated by the Ambegaokar-Halperin theory for a single overdamped junction at finite temperature[15]) and so the pulselike jumps in $R(f)$ become more rounded. This is the basic explanation for the behavior of our data in Fig. 3.

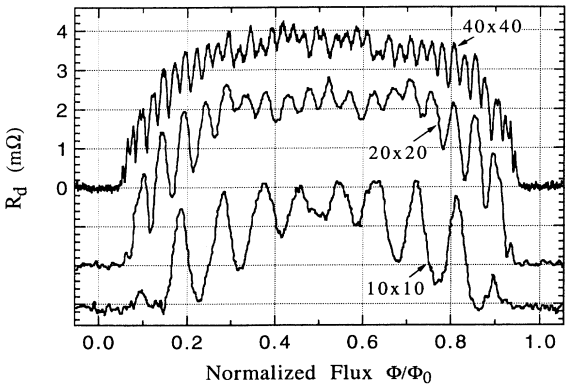


FIG. 3. Measured $R_d(f)$ at 1.6 K (where $\beta=0.08$) for a 10×10, 20×20, and 40×40 plaquette hybrid array. The maxima in $R_d$ occur at $f=n/11$, $n/21$, and $n/41$ for the three arrays, with $n$ an integer, as expected for a 11, 21, or 41 junction interferometer.

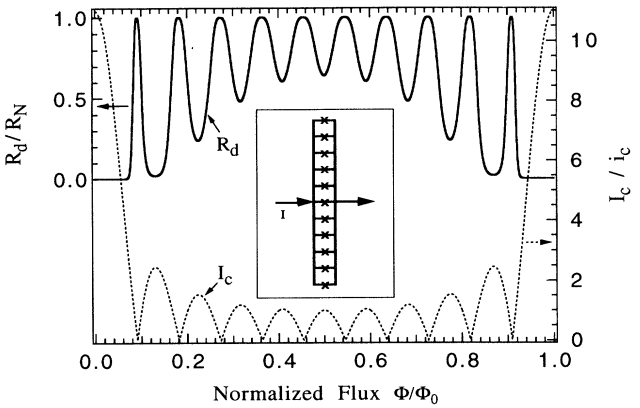


FIG. 4. Computed $I_c(f)$ (dotted) and $R_d(f)$ (solid) plots for an 11-junction interferometer. The $R_d(f)$ curve was obtained using the Ambegaokar-Halperin expression for $V(I/I_c;I_c/T)$ for a single junction (see text for details).

We can use the above explanation to calculate the expected behavior of $R_d(f)$ for an 11-junction interferometer, as shown in the solid curve in Fig. 4. Using $I_c(f)$ from Eq. (6), the field-dependent $dV/dI$ was derived from the Ambegaokar-Halperin form for $V(I/I_c;I_c/T)$. We have taken $I/I_{c0}=0.045$ [where $I_{c0}=I_c(f=0)$] to approximate our experimental ac bias current $I_{\rm bias}\approx i_c/2$. The ratio $I_{c0}/T$ was obtained from fits[16] of the zero-field experimental $R_d(I)$ curves at 1.6 K to the Ambegaokar-Halperin theory. Although this theory was intended for a single junction we find that it works reasonably well in fitting the array $R_d(I)$ curves for $f=0$. For simplicity we maintain this form as an approximation for $R_d(I)$ at all fields. Using this procedure our calculated behavior for $R_d(f)$ (solid curve in Fig. 4) provides a good description of the experimental data for the 10 plaquette by 10 plaquette array at 1.6 K presented in Fig. 3 (bottom curve), with an accurate rendering of the oscillation positions and amplitudes.

The 20×20 and 40×40 arrays (Fig. 3) show the same type of oscillation of $R_d(f)$, but the oscillation amplitude relative to the overall background modulation decreases with array size. For data on the 400×400 arrays (not shown), there is only a smooth background variation in $R_d$ between integral values of $f$; the interferometer oscillations are too weak to resolve. From the excellent agreement between the $R_d(f)$ measurements on the hybrid arrays (Fig. 3) and the calculated $R_d(f)$ for a 1D interferometer (Fig. 4), we conclude that when $\beta\ll 1$, each column of the hybrid array is decoupled from neighboring columns and behaves like an $N$-junction interferometer. The overall behavior of the array is just that of $(N-1)$ independent identical interferometers in series.

Figure 5 shows several measured $R_d(f)$ curves for the 20×20 array as the temperature decreases (and thus as $i_c$ and $\beta$ increase). The 1.6 K data are the topmost plot and subsequent curves were obtained by lowering the temperature in 0.1 K intervals. [As a basis for comparing the $R_d(f)$ curves at different temperatures, we kept the maximum of $R_d$ at each temperature at about 2 mΩ using a

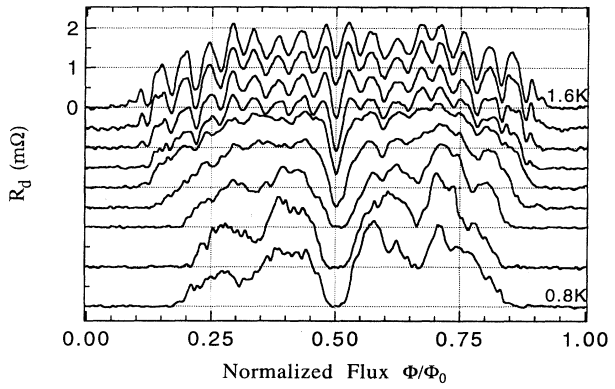


FIG. 5. Measured $R_d(f)$ curves for a $20\times20$ plaquette hybrid array at different temperatures (at 0.1 K intervals). At 1.6 K (top curve, corresponding to $\beta=0.08$) the features are those of an 11-junction interferometer, while at 0.8 K (bottom curve, corresponding to $\beta=0.96$), the structure shows only the signatures of low-order commensurate states at $f=1/2$, 1/3, 2/3.

variable dc offset current.] As the temperature is lowered, there is a qualitative change in the structure of the $R_d(f)$ curve. The interferometer oscillations gradually decrease in amplitude, while there is a simultaneous development of broad, deep minima at the most strongly commensurate fields ($f=1/2$, 1/3, and 2/3). For $T\leq1$ K ($\beta\geq0.6$), the interferometer behavior has almost entirely disappeared, leaving only the commensurate field structure. We have also observed the same behavior on the $10\times10$ array with somewhat less pronounced minima at $f=1/3$ and $f=2/3$.

We have already described how for $\beta\ll1$ the hybrid arrays are well modeled by a 1D interferometer. However, the low-temperature curves in Fig. 5 (where $\beta$ is of order 1) are typical of data found for a standard 2D square Josephson junction array.[17] We are now faced with an obvious question: what drives the crossover from the small $\beta$ (high temperature) behavior characteristic of 1D systems to the $\beta\approx1$ (lower temperature) results typical of 2D systems?

At sufficiently high temperatures, the junctions' small critical currents yield $L_J=\Phi_0/2\pi i_c\gg L_g$. It follows from Eq. (4) that the phase gradients induced along the wires ($\sim L_g I$) are then negligible compared to those across the junctions ($\sim L_J I$). In this limit, the only phase drops present around each plaquette will be across the junctions themselves, and the hybrid array will be topologically equivalent to ideal interferometers in series.

At lower temperatures, the marked increase in $i_c$ leads to $L_J\approx L_g$, in which case the phase differences across the junctions and wires are comparable. This situation in which phase drops can occur along all four sides of each plaquette (two with junctions, two without) is topologically equivalent to a (possibly anisotropic) 2D square Josephson-junction array. For this reason, the observed experimental crossover from the high-temperature 1D behavior to the low-temperature 2D behavior can be attributed to the development of significant phase gradients along the wires at low temperatures. We will discuss these ideas at greater length in Sec. VI, but first we present the results of numerical studies which lend further support to the hypothesis just outlined.

## V. SIMULATIONS

The previous section concluded with a description of the hybrid arrays which suggests that they may be fruitfully modeled as anisotropic square Josephson-junction arrays (i.e., anisotropic $XY$ systems), using different Josephson coupling strengths in the two perpendicular directions. Since phase drops arise from current flow when *inductances* are present in the system [see Eq. (4)], replacing the wires by junctions with Josephson inductance $L_{J,y}$ is simply an approximation by which we can substitute a junction inductance $L_{J,y}=\Phi_0/2\pi i_{c,y}$ for the wire's geometric inductance $L_g$. Let us define the junction direction as $x$ and the direction parallel to the superconducting wires as $y$. In our $XY$ model, the junction critical currents in the $x$ and $y$ directions are $i_{c,x}=\Phi_0/2\pi L_{J,x}$ and $i_{c,y}=\Phi_0/2\pi L_{J,y}$. The high-temperature interferometer limit of the hybrid array corresponds to the extremely anisotropic limit in which the anisotropy ratio $\alpha=L_{J,x}/L_{J,y}=i_{c,y}/i_{c,x}$ diverges, and the crossover to the 2D arrays is expected as $\alpha$ approaches unity (in this model $\alpha$ corresponds to $1/\beta$). We should stress that *for our experimental system* it is the anisotropy of the *inductances* in the two perpendicular directions, *not the critical currents,* which dictates the anisotropy in the phase drops. The critical current of the wires is still much larger than the junction $i_c$'s even at the lowest temperatures studied and plays no significant role in the behavior of the system.

The simulated arrays consist of $N\times M$ superconducting nodes. Current is injected via superconducting bus bars connected to the edge nodes by junctions with critical current $i_{c,x}$.[18] These simulations were made using the overdamped resistively shunted junction model to describe the junctions. As in earlier simulations[19] we solve the coupled differential equations obtained from current conservation at each node. The current $i_{ab}$ from node $a$ to a neighboring node $b$ is

$$i_{ab}=i_c\sin\left[\varphi_b-\varphi_a-\frac{2\pi}{\Phi_0}\int_a^b\mathbf{A}\cdot d\mathbf{l}\right]+\frac{V_{ab}}{R_N}\,, \tag{7}$$

where

$$V_{ab}=\frac{\hbar}{2e}\frac{d}{dt}(\varphi_b-\varphi_a) \tag{8}$$

is the voltage across the junction between nodes $a$ and $b$, $\varphi_a(\varphi_b)$ is the phase of node $a$ ($b$), $R_N$ is the normal-state junction resistance, and $\mathbf{A}$ is the vector potential. We use the London gauge $\mathbf{A}=Hx\hat{y}$ so that the integral $\int_a^b\mathbf{A}\cdot d\mathbf{l}$ is nonzero only for paths along the $y$ direction, in which case it equals $2\pi Hx_a(y_b-y_a)/\Phi_0$, where $y_b(y_a)$ is the $y$ coordinate of node $b$ ($a$) and $x_a$ is the $x$ coordinate of node $a$. Current conservation at node $a$ yields

$$\sum_b i_{ab}=0 \tag{9}$$

for all nodes except the bus bars, where the sum of the currents is equal to the externally applied current.

Equations (7)–(9) give $(N\times M)+1$ coupled first-order differential equations (the phase of the left bus bar can be arbitrarily chosen to be 0) for the phases as a function of time. We use free boundary conditions. Starting with a given phase configuration we integrate the phases forward in time using a fourth-order Runge-Kutta method with adaptive step size[20] (the time step size is adjusted at each integration step to be the largest that will maintain a truncation error estimate on the phases of less than $10^{-4}$ radians). For a given dc current and magnetic field, we let the phases relax for 500 time constants $\tau=\hbar/2ei_{c,x}R=L_{J,x}/2R$ before averaging the voltage for 200 time constants. To find $I_c(f)$ we define $I_c$ to be the current for which the normalized voltage per junction $V/i_cR_N$ first exceeds 0.02, and compute $I_c$ using the van Wijngaarden-Dekker-Brent zero-crossing method[20] at each field.

Figure 6 shows the computed $I_c(f)$ for three different anisotropy ratios $\alpha$ for an 11 node by 11 node array (10 by 10 plaquette). For an anisotropy of $\alpha=20$, $I_c$ displays the structure expected for an 11-junction interferometer, namely that of Eq. (6) with $N=11$. As the anisotropy is decreased to $\alpha=5$ the critical current is generally enhanced compared to the more anisotropic case, and the amplitude of the oscillations of $I_c(f)$ decreases. When the system is isotropic ($\alpha=1$), $I_c$ exhibits a strong maximum at $f=1/2$ and weaker maxima at $f=1/3$ and 2/3, as is expected for a 2D array, while the interferometer structure has completely disappeared (in Fig. 6 the $\alpha=1$ and $\alpha=5$ curves have been vertically offset by $0.1Ni_c$).

An examination of the computed phase drops along the junctions in the two directions in the presence of a noninteger field and in the absence of a transport current shows a marked change as the anisotropy is increased. For the isotropic system the magnitude of the phase drops in the $x$ and $y$ directions is the same on average. As the anisotropy ratio is increased the phase drops become smaller along the $y$ direction and consequently larger along the $x$ direction [since the directed sum of the phases around any plaquette must be equal to $2\pi f$ modulo $(2\pi)$]. For an anisotropy as large as 20, the phase drops are essentially all in the $x$ direction. For example, when $f=1/2$ the magnitude of the phase change along $y$ is at most 0.03 radians per junction rather than $\pi/4$ radians found for the isotropic case.

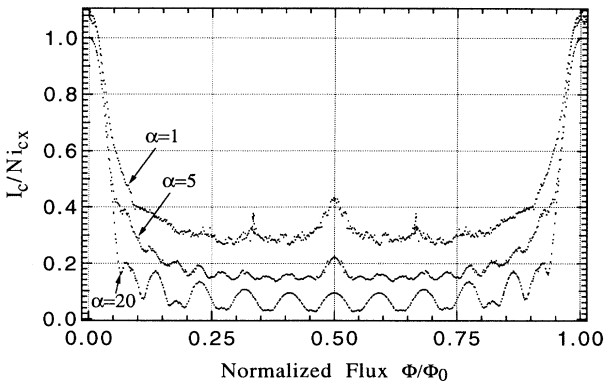


FIG. 6. Simulated $I_c(f)$ curves for an anisotropic array of 11 by 11 Josephson junctions (10 by 10 cells). The three plots correspond to anisotropy ratios $\alpha$ of 20, 5, and 1 (the $\alpha=5$ and $\alpha=1$ plots are vertically offset by $0.1Ni_c$).

## VI. DISCUSSION

Let us first consider the case of no screening so that the magnetic field is uniform (this corresponds to $\beta=0$). For a $N$-junction interferometer with identical junctions, the current through the device is given by Eq. (5). Again, $I_c$ is found by maximizing $I$ with respect to $\gamma_0$. If $f$ is commensurate ($f=p/q$ with $p$ and $q$ integers), the phase pattern repeats every $q$ cells. It is easily shown that the net supercurrent through the $q$ junctions of such a supercell vanishes:

$$i_c\sum_{n=1}^{q}\sin(\gamma_0+2\pi np/q)=0\ . \tag{10}$$

Thus, for commensurate fields, the transport current through the interferometer is essentially an edge effect due to excess cells at one edge which do not form a complete supercell. In general (for $p\neq q$), $I_c(f=p/q)/i_c<q$ [and $I_c(f)/i_c\leq N$], and commensurate fields are not necessarily accompanied by maxima in $I_c$. Furthermore, in the thermodynamic limit of large $N$, only integer $f$ give nonzero $I_c/N$.

Let us look more closely at the case of $f=1/2$. If the number of junctions $N$ is even, then $I_c=0$ for any choice of $\gamma_0$. For odd $N$, $\gamma_0=\pi/2$ results in all even junctions having a phase drop $\gamma=\pi/2$ and all odd junctions having $\gamma=3\pi/2$; the resulting $I_c$ is just the critical current $i_c$ of the single uncompensated junction which is not part of a two-junction supercell.

We now turn to the case where each cell has a self-inductance $L_g$. $\beta$ is no longer zero and there can now be current induced phase gradients along the wires proportional to $L_gI$. For $f=1/2$ the induced flux per cell will alternate between $\Delta\Phi$ and $-\Delta\Phi$, reflecting the vortex pattern, and $I$ becomes [adapting Eq. (5) to account for nonuniform flux]:

$$I=i_c\sin(\gamma_0)+i_c\sum_{n=1}^{N-1}\sin\left[\gamma_0+\sum_{j=1}^{n}\left[\pi+(-1)^j\frac{2\pi\Delta\Phi}{\Phi_0}\right]\right]\ . \tag{11}$$

$I$ is now maximized for even $N$ by choosing $\gamma_0=\pi\Delta\Phi/\Phi_0$. The resulting $I_c$ scales with $N$:

$$\frac{I_c}{i_c}=N\sin\left[\frac{\pi\Delta\Phi}{\Phi_0}\right]\ . \tag{12}$$

(A similar result can be obtained for odd $N$.) This simple illustration, for which only self-inductances have been considered, shows how a single row of Josephson junctions can display a 2D-like enhancement of $I_c$ at $f=1/2$ if there are phase variations along the wires connecting the junctions. Commensurate states other than $f=1/2$ can be similarly shown to give rise to $I_c\propto N$.

Numerical calculations of $I_c(f)$ for a ten-junction interferometer, taking self- and mutual inductances into account, have been performed by Miller *et al.*[7] Assuming uniform current injection, they observed that as $\beta=L_g/L_J$ is increased, in addition to the standard ten-junction interferometer $I_c(f)$ behavior there also appears a maximum at $f=1/2$, replacing the minimum present in the zero-inductance case ($\beta=0$), as well as possible maxima at other commensurate $f$. This observation supports our simple argument presented above. [Bock *et al.*[6] have carried out a more exact calculation including mutual inductances for a nine-junction interferometer with an asymmetric current injection in which the current is injected on one wire and extracted from the other wire on the same side of the array. Their data show no enhancement of $I_c$ at commensurate fields as $\beta$ is increased, but this is related to the asymmetric current injection.[21]]

To obtain quantitative values for the loop inductance $L_g$ of a single hybrid array cell, we can model it as a square superconducting washer with a square hole of side 8 $\mu$m and wire width 2 $\mu$m. Using the results of Jaycox and Ketchen,[22] we find for our geometry $L_g=15$ pH. Using this value, we find $\beta=L_g/L_f$ increases from $\beta=0.08$ at 1.6 K (where $i_c=1.7$ $\mu$A) to $\beta=0.96$ at 0.8 K (where $i_c=21$ $\mu$A).

We can also calculate the induced phase drop $\gamma_{\rm ind}$ around each loop of inductance $L_g$ in which a current $I$ is flowing:

$$\gamma_{\rm ind}=2\pi\frac{L_g I}{\Phi_0} . \tag{13}$$

Since the current in the wires (in a noninteger field) will be of order $i_c$, we can "tune" the maximum possible phase drop occurring along the wires of the hybrid arrays by changing the critical current of the junctions. In fact, since $\beta=L_g/L_J$, we can see that $\gamma_{\rm ind}=\beta\cdot i/i_c=\beta\sin(\gamma_J)=\beta[\gamma_J+O(i/i_c)^3]$. So for $i/i_c\ll 1$ we have $\gamma_{\rm ind}/\gamma_J\approx\beta$. As $\beta$ approaches 1 (where commensurate states typical of 2D arrays are clearly seen) phase differences along the wires and across the junctions are of the same order, whereas when $\beta\approx 0$ [where interferometer (1D) structure is observed] virtually all the phase differences occur across the junctions.

In our simulations of 2D anisotropic arrays, we observed a similar crossover from 1D to 2D behavior (i.e., from the absence to the presence of commensurate states) as the anisotropy of the system was reduced. With an anisotropy ratio of $\alpha=5$ corresponding to $\beta=0.2$, we found that the interferometer structure had substantially decayed, while the maximum in $I_c(f)$ at $f=1/2$ became more pronounced (see Fig. 6). In Fig. 5, the experimental data taken at 1.2 K is comparable in the nature of its structure (interferometer behavior fades as the $f=1/2$ extremum strengthens), and at this temperature $\beta\sim 0.3$. This very reasonable agreement implies that the replacement of the hybrid array wires by junctions for the purposes of simulating inductively induced phase differences is a valid approach, at least for our geometry. We should point out that this procedure provides a means for incorporating the array cell self-inductances but does not account for mutual inductance effects. The sufficiency of this method for computing critical currents is plausible given that Phillips *et al.*[5] have shown that the inclusion of self-inductances alone is adequate for describing *static* array properties (such as the cell-cell energy barrier for fluxon motion).

## VII. CONCLUSIONS

With the goal of studying superconducting arrays in the limit of extreme anisotropy, we have fabricated devices with a new hybrid square geometry consisting of weak-link junctions in one direction and superconducting wires in the perpendicular direction. Measurements of the dynamic resistance as a function of field displayed qualitatively different behavior in two different temperature regimes: the system displays 1D behavior identical to $N$-junction interferometers at higher temperatures, while the characteristic signature of 2D arrays is found at lower temperatures. We have shown that this crossover is mainly dictated by the significance of array loop geometric self-inductances $L_g$ relative to the Josephson inductances $L_J$ of the weak links. Both experiments and numerical simulations have demonstrated this dimensionality crossover when $\beta=L_g/L_J=2\pi L_g i_c/\Phi_0$ is approximately 0.3.

The key to understanding this crossover seems to lie in the topology of the phase gradients in the system. For the hybrid arrays, when $\beta\ll 1$, the only significant phase changes occur across the junctions. This effectively decouples each column of junctions from its neighboring columns, and so the behavior of the system is essentially one dimensional. As $\beta$ approaches 1, significant phase gradients are set up along the wires as well, resulting in 2D coupling throughout the array. We have simulated this behavior numerically using an anisotropic $XY$ model where phase drops across weak links in one of the two perpendicular directions were used as an approximation for the current-induced phase gradients along the wires of the experimental system. The good agreement between the experimental and numerical data attests to the validity of this approach.

## ACKNOWLEDGMENTS

We wish to thank Richard J. Fitzgerald for his considerable help with the numerical simulations as well as for his assistance with the measurements. We also thank John Free for advice regarding the simulations and the Harvard VLSI group for the use of their computers. H.R.S. acknowledges support of a NSERC of Canada fellowship. This research was supported in part by ONR Grant No. N00014-89-J-1565, JSEP Grant No. N00014-89-J-1023, and NSF Grant No. DMR-92-07956.

[1]Wei-min Zhang, W. M. Saslow, and M. Gabay, Phys. Rev. B **44**, 5129 (1991); W. M. Saslow, M. Gabay, and W.-M. Zhang, Phys. Rev. Lett. **68**, 3627 (1992).

[2]B. Berge, H. T. Diep, A. Ghazali, and P. Lallemand, Phys. Rev. B **34**, 3177 (1986).

[3]C.-R. Hu and M. Niu, Bull. Am. Phys. Soc. **38**, 803 (1993); Ming Niu, Ph.D. thesis Texas A&M University, 1993.

[4]M. A. Itzler, R. Bojko, and P. M. Chaikin, Europhys. Lett. **20**, 639 (1992); M. A. Itzler, G. M. Danner, R. Bojko, and P. M. Chaikin, Phys. Rev. B **49**, 6815 (1994).

[5]J. R. Phillips, H. S. J. van der Zant, J. White, and T. P. Orlando, Phys. Rev. B **47**, 5219 (1993).

[6]R. D. Bock, J. R. Phillips, H. S. J. van der Zant, and T. P. Orlando, Phys. Rev. B **49**, 10 009 (1994).

[7]J. H. Miller, Jr., G. H. Gunaratne, J. Huang, and T. D. Golding, Appl. Phys. Lett. **59**, 3330 (1991).

[8]A. Majhofer, T. Wolf, and W. Dieterich, Phys. Rev. B **44**, 9634 (1991).

[9]L. L. Sohn, M. T. Tuominen, M. S. Rzchowski, J. U. Free, and M. Tinkham, Phys. Rev. B **47**, 975 (1993).

[10]S. Teitel and C. Jayaprakash, Phys. Rev. Lett. **51**, 1999 (1983).

[11]R. Rammal, T. C. Lubensky, and G. Toulouse, Phys. Rev. B **27**, 2820 (1983).

[12]P. G. De Gennes, Rev. Mod. Phys. **36**, 225 (1964).

[13]C. M. Falco, W. H. Parker, S. E. Trullinger, and P. K. Hansma, Phys. Rev. B **10**, 1865 (1974).

[14]We do not fully understand the small asymmetry in the peak heights in Fig. 2, but our main concern is with the peak locations (i.e., the critical currents), and these are symmetric to within 2%.

[15]Vinay Ambegaokar and B. I. Halperin, Phys. Rev. Lett. **22**, 1364 (1969).

[16]The fit gave $I_{c0}/T=0.85$ $\mu$A/K, while the experimental values for $I_{c0}$ and $T$ yielded $I_{c0}/T=13.7$ $\mu$A/K. Fits to the Ambegaokar-Halperin expression gave the same $I_{c0}/T$ ratio for $10\times10$, $20\times20$, and $40\times40$ arrays, despite the fact that the array critical current scaled with array size in those three cases. It is interesting to note that the $I_{c0}/T$ ratio obtained from the fits (0.85 $\mu$A/K) is close to $i_c/T=1.06$ $\mu$A/K, where $i_c$ is the single junction critical current, suggesting that the thermal broadening of the $I$-$V$ curves is dictated by fluctuations of independent single junctions.

[17]S. P. Benz, M. S. Rzchowski, M. Tinkham, and C. J. Lobb, Phys. Rev. B **42**, 6165 (1990).

[18]In the simulations current is injected and extracted via bus bars rather than from two opposite corners of the array as in the experimental setup. Bus bars are used because our simulations include the isotropic case for which the corner injection scheme leads to a strong reduction in $I_c(I_c \leq 2i_c)$ compared to the $I_c \leq Ni_c$ result obtained using the bus bar configuration.

[19]S. R. Shenoy, J. Phys. C **18**, 5163 (1985); K. K. Mon and S. Teitel, Phys. Rev. Lett. **62**, 673 (1989); J. S. Chung, K. H. Lee, and D. Stroud, Phys. Rev. B **40**, 6570 (1989); J. U. Free, S. P. Benz, M. S. Rzchowski, M. Tinkham, C. J. Lobb, and M. Octavio, Phys. Rev. B **41**, 7267 (1990).

[20]W. Press, B. Flannery, S. Teukolsky, and W. Vetterling, *Numerical Recipes* (Cambridge University Press, Cambridge, 1988).

[21]H. S. J. van der Zant (private communication).

[22]J. M. Jaycox and M. B. Ketchen, IEEE Trans. Magn. **MAG-17**, 400 (1981).